Determination of the Thin Film Structure of Zwitterion Doped Poly(3,4-ethylenedioxythiophene):Poly(styrenesulfonate). A Neutron Reflectivity Study

Gabriel E. Pérez,*,† Gabriel Bernardo,‡ Hugo Gaspar,‡ Joshaniel F.K. Cooper,¶ Francesco Bastianini,† Andrew J. Parnell,‡ and Alan D.F. Dunbar*,†

†*Department of Chemical and Biological Engineering, The University of Sheffield, S1 3JD, UK*

‡*Department of Physics and Astronomy, The University of Sheffield, S3 7RH, UK*

¶*ISIS Pulsed Neutron and Muon Source, STFC, Rutherford Appleton Laboratory, OX11 0QX, UK*

E-mail: geperez1@sheffield.ac.uk; a.dunbar@sheffield.ac.uk

Phone: +44 114 222 7555; +44 114 222 7551

Abstract

Doping poly(3,4-ethylenedioxythiophene):poly(styrene sulfonate) (PEDOT:PSS) is known to improve its conductivity, however little is known about the thin film structure of PEDOT:PSS when doped with an asymmetrically charged dopant. In this study, PEDOT:PSS was doped with different concentrations of the zwiterion 3-(N,N Dimethylmyristylammonio)propanesulfonate (DYMAP), and its effect on the bulk structure of the films characterized by neutron reflectivity. The results show that at low doping concentration, the film separates into a quasi bi-layer structure with lower roughness

(10%), increased thickness (18%), and lower electrical conductivity compared to the undoped sample. However when the doping concentration increases the film forms into a homogeneous layer and experiences an enhanced conductivity by more than an order of magnitude, a 20% smoother surface, and a 60% thickness increase relative to the pristine sample. Atomic force microscopy and profilometry measurements confirmed these findings, and AFM height and phase images showed the gradually increasing presence of DYMAP on the film surface as a function of the concentration. Neutron reflectivity also showed that the quasi bi-layer structure of the lowest concentration doped PEDOT:PSS is separated by a graded rather than a well defined interface. Our findings provide an understanding of the layer structure modification for doped PEDOT:PSS films that should be prove important for device applications.

Keywords

PEDOT:PSS, conductivity, zwitterion, film structure, neutron reflectivity, hole transporting layer

1 Introduction

Poly(3,4-ethylenedioxythiophene) polystyrene sulfonate (PEDOT:PSS) is arguably the most commonly used hole transporting layer (HTL) material in organic solar cells (OSC).[1,2] This is due to its high transparency to most of the solar spectrum when processed as a thin film,[3] good mechanical and thermal stability,[4–6] and excellent water solubility.[7] In addition to this, it has low toxicity and a high work function which allows it to make a good ohmic contact with polymer donors.[8] These characteristics make it a good hole transporter and electron blocking material.[9] However, PEDOT:PSS is far from being optimised for OSCs and therefore significant potential still exists to increase the performance. Several types of additives have been mixed with PEDOT:PSS, in order to improve its hole transporting properties

in OSCs, specifically by improving its electrical conductivity[10]. These additives include polar solvents[11,12], alcohols[13,14], ionic liquids[15], polyelectrolytes[16] acids[17,18], surfactants[19], salts[20–23], and zwitterions[24,25]. The inclusion of these asymmetrically charged additives into PEDOT:PSS causes a variety of complex morphological changes in its molecular structure. For example, the increase in conductivity of PEDOT:PSS by doping it when in aqueous dispersion (solvent doping) has been widely interpreted as a result of the weakening of the Coulombic attractions between the positively charged conducting PEDOT and the negatively charged insulating PSS moieties induced by the dual-charge dopant[20–28]. This is argued to result in a phase separation between the two moieties which causes a conformational change of the originally entangled PEDOT and PSS chains[20,23,28] to a more ordered conducting network that facilitates improved charge transport[29] when deposited as a thin film. While this is a widely accepted theory in the field, this change in morphology has been mostly studied using surface techniques rather than as a thin film due to the fact that most bulk techniques are not very sensitive to disordered polymer blends composed of two materials close in nature (i.e. PEDOT and PSS). The lack of a more precise understanding about how these changes occur has caused ambiguity and inconsistencies in the literature, hindering progress in understanding the effect additives have on the morphology of PEDOT:PSS thin films. For instance, the mechanisms of morphology change described above assume that there is a homogeneous merging of the additive with the PEDOT:PSS in solution that persists during film deposition and formation. Hence the possibility of a non uniform distribution of the additive within the deposited thin film has not been considered, even though the separation of organic compounds within the bulk of a mixture is a common phenomenon during the preparation or the treatment of the film or the device that the film is part of.[30,31] Therefore, it is necessary to develop a deeper understanding of the mechanisms of conductivity improvement and morphological changes caused by the use of additives, in order to achieve a significant improvement in PEDOT:PSS engineering. This work was specifically conducted to determine if a PEDOT:PSS solution doped with an asymmetrically charged dopant results

in a homogeneous single layer or a multi-layer structured film after deposition.

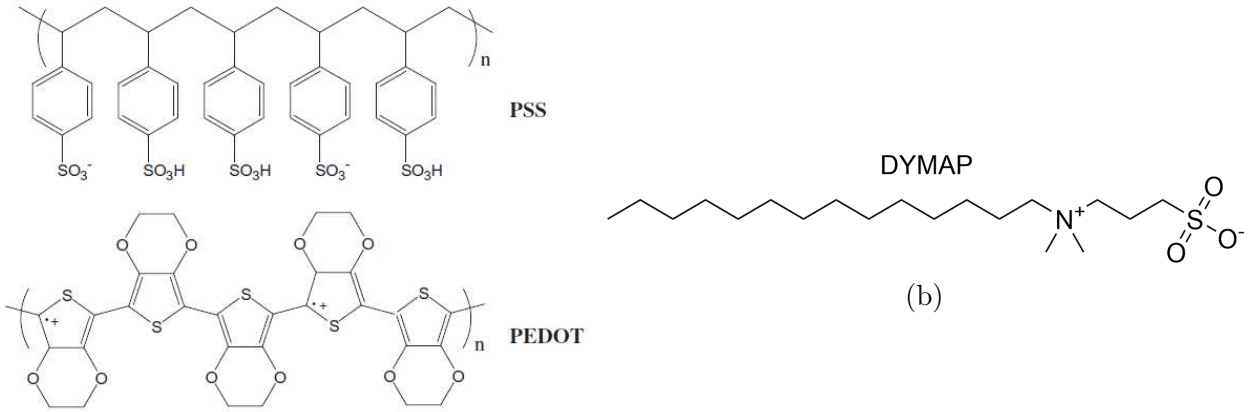

Figure 1: *Chemical structures of (a) PEDOT:PSS and (b) DYMAP.*

Neutron scattering techniques can provide detailed information about the nanoscopic behaviour of condensed matter. They differ from other scattering techniques such as X-rays or light scattering in the fact that neutrons scatter from materials by interacting with the nucleus of an atom rather than the electron cloud. This makes a neutron beam a non-destructive and highly penetrating probe useful to study bulk morphologies without altering the chemistry of high-energy sensitive samples such as organic molecules. Specular neutron reflectivity (NR) is a technique that can provide information about the homogeneity of a thin film normal to a surface. Although neutron scattering techniques have been used in the past to study the morphology of PEDOT:PSS and its interactions with other compounds[32–34] , to the best of our knowledge neutron scattering techniques have yet to be used to study the bulk morphological change and electrical conductivity enhancement of zwitterion doped PEDOT:PSS.

In this work we used the zwitterion 3-(N,N Dimethylmyristylammonio)propanesulfonate (DYMAP) Figure 1 to dope a PEDOT:PSS aqueous dispersion (1:2.5 ratio, commonly used for organic light emitting diodes and OSCs applications) at three different concentrations (0 mM, 10 mM, and 20 mM) to spin cast thin films similar to the ones used in OSC. We measured the electrical conductivity to identify the concentration at which the expected change

in morphology occurs (indicated by an abrupt change in conductivity). We then used NR to study the thin film structure and discuss the characteristics and homogeneity of the resultant films. We also conducted atomic force microscopy (AFM) and profile (profilometer) measurements to determine roughness and thickness of the films respectively. This information was used to confirm and constrain the parameters of the NR data modelling and allowed us to further understand the surface morphology of the films. Finally we incorporated the films into photovoltaic devices based on a Poly[N-9'-heptadecanyl-2,7-carbazole-alt-5,5-(4'7'-di-2-thienyl-2',12,32-benzothiadiazole)] (PCDTBT): [6,6]-Phenyl-C71-butyric acid methyl ester ($PC_{71}BM$) blend as the active layer to determine the effect of dopant concentration for doped HTLs on the photovoltaic performance of OSC devices.

2 Results and discussion

2.1 Electrical Conductivity

The electrical conductivity of PEDOT:PSS is dependant on its morphology which can be modified by an asymmetrically charged dopant that alters the electrostatic interactions between PEDOT and PSS. Therefore a good indicator that a morphological change has occurred within doped PEDOT:PSS is a drastic change in its conductivity. Our first motivation to measure the conductivity of DYMAP doped PEDOT:PSS films was to corroborate that DYMAP would increase the conductivity of PEDOT:PSS. We also wanted to find the doping concentrations at which DYMAP has not yet drastically altered the conductivity of PEDOT:PSS, and the one at which it does. This would suggest that a relevant morphological change has occurred and motivate us to use NR to study those concentrations. Conductivity was calculated by measuring the sheet resistance and thickness of the films straight after annealing to minimize any swelling of the films due to ambient water absorption (see discussion in supporting information S-2 to S-3). The conductivity results are shown in table 1.

Table 1: *Conductivities of pristine, 10, and 20 mM doped PEDOT:PSS as a function of doping concentration.*

Doping concentration	Conductivity (S cm^{-1})
Pristine PEDOT:PSS	(2.7 ± 0.3) x 10^{-2}
10 mM DYMAP doped PEDOT:PSS	(1.5 ± 0.3) x 10^{-2}
20 mM DYMAP doped PEDOT:PSS	0.8 ± 0.4

These results are interesting since we expected that the conductivity would improve as the concentration of DYMAP in PEDOT:PSS increased, in line with other cases in literature in which PEDOT:PSS is doped with an asymmetrically charged dopant.[11,20,26] The conductivity of pristine PEDOT:PSS was (2.7 ± 0.3) x 10^{-2} S cm^{-1}, slightly higher than the 10 mM doped sample which had a conductivity of (1.5 ± 0.3) x 10^{-2} S cm^{-1}. However, when the doping concentration was further increased to 20 mM, the conductivity increased to 0.8 ± 0.4 S cm^{-1}, more than one order of magnitude higher compared to the pristine sample. As mentioned before, the increase in conductivity of PEDOT:PSS induced by the doping of an asymmetrically charged molecule such as DYMAP has been attributed to reduction of the coulombic attractions between PEDOT and PSS. This is caused by a screening effect produced by the dopant which has been argued to enhance the hopping rate of charge carriers within the film.[35,36] Additionally, the dramatic increase in conductivity from the 10 mM doped film to the 20 mM doped one is indicative of a percolation threshold being crossed. Such phenomenon is worth investigating in a separate study.

These conductivity results imply that a significant conformational change in the morphology of PEDOT:PSS[10,24,29] is likely to be ocurring as the DYMAP doping concentration is increased from 10 mM to 20 mM.

2.2 Neutron Reflectivity

After determining the concentrations at which the DYMAP induced a significant change in the electrical conductivity of PEDOT:PSS, we conducted NR on the pristine (0 mM), 10 mM, and 20 mM DYMAP doped samples to study their film structures. Figure 2a shows the

NR data for a pristine PEDOT:PSS sample and the model used to fit it. A stack consisting of three layers was required for the model (see figure 2b). From bottom to top these layers were silicon (Si) substrate, a silicon oxide (SiO_2) layer, and the PEDOT(1):PSS(2.5) film. For each layer three parameters were considered in the model. These were thickness (D), root mean square roughness (σ_{RMS}), and scattering length density (SLD).

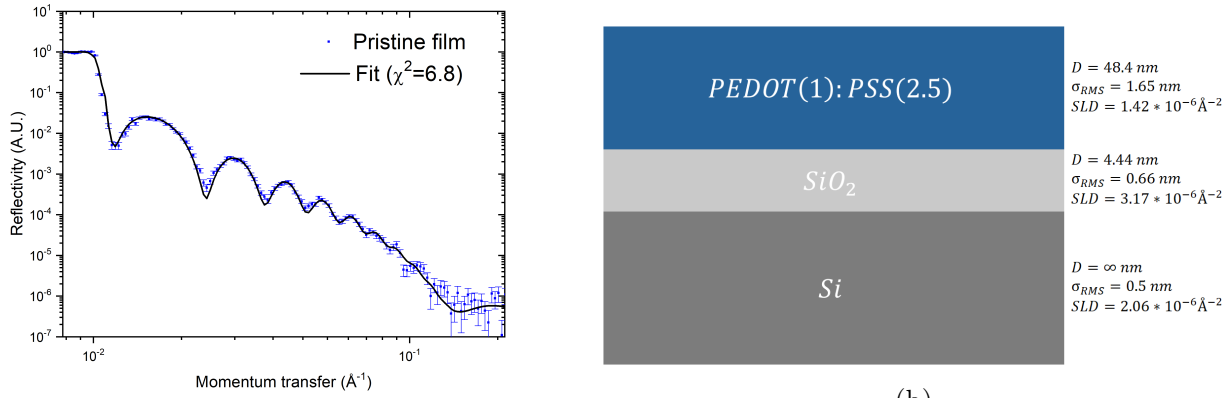

(a) (b)

Figure 2: *(a) Neutron reflectivity data for the pristine PEDOT:PSS film and its corresponding fit. (b) Sketch of the stack proposed for the model (not to scale) along with their respective fit values for thickness (D), root mean square roughness (σ_{RMS}), and scattering length density (SLD)*

While the three parameters of the Si layer were fixed to well known SLD values, the parameters for the SiO_2 layer were all fitted. The thickness of the fitted layer was 4.44 nm. This is slightly high for a native oxide which typically has a thickness between 1 and 3 nm. In order to corroborate this layer was native oxide we removed the polymer layers from the substrate and conducted ellipsometry and AFM. We concluded that it is in fact an accurate thickness for the native oxide (see supporting information S-2 to S-3). Since this particular substrate came from a different batch and was cleaned with a different process than the other substrates used in this study it is not so surprising that the oxide layer had a different thickness. Moreover, the σ_{RMS} of the SiO_2 layer was 0.66 nm and its SLD was 3.17×10^{-6} Å^{-2} both within the known values for this material.

The NR simulation of the PEDOT:PSS layer resulted in a 48.4 nm thick film which was as expected for the spin coating conditions used to deposit the polymer (4000 RPM, 40 s),[37]

very similar to the 48 nm measured by the profilometer. The root mean square roughness (σ_{RMS}) of the film was 1.65 nm which is similar to the 1.19 nm resulting σ_{RMS} from the AFM measurement conducted on the same film. The SLD for this particular PEDOT:PSS composition (1:2.5 ratio) was unknown so it was also fitted and the resulting value was 1.42×10^{-6} Å^{-2} which is very similar to the 1.68×10^{-6} Å^{-2} of the more conventional PEDOT:PSS formula (1:6 ratio) reported in the literature.[38] To further confirm the validity of this SLD value, we calculated the theoretical SLD values for the EDOT and PSS monomers which are 1.8×10^{-6} Å^{-2} and 1.57×10^{-6} Å^{-2} respectively. These values are slightly higher than the SLD value obtained from the fit. Since we measured the samples more than 24 hours after their preparation to allow stabilization of water absorption, and the SLD H_2O is -5.61×10^{-6} Å^{-2} we attributed the lower than expected SLD of the PEDOT:PSS film, i.e. compared to that of the separate monomers, to the presence of water molecules absorbed in the film due to the highly hygroscopic nature of PEDOT:PSS.

In order to determine if there is a bi-layer structure within PEDOT:PSS:DYMAP after spin-coating, two different models were tested for the 10 mM sample. Then we compared the probabilistic evidence of the two models using χ^2 as the normalisation constant for both models to determine the most probable structure of films. As suggested by Sivia and Webster[39] a significant change in the probabilistic evidence is strong evidence that the model with the lowest normalistaion constant is the most accurate description for the structure that is being analyzed. Both models consisted of a 10 mM doped PEDOT:PSS film on top of a silicon substrate and a native oxide, however for one model the polymer film was split into two layers, and for the other model the polymer film was simulated as one homogeneous layer. Figure 3 shows the NR data of the 10 mM doped sample along with fits of the two models all plotted as reflectivity multiplied by the Fresnel decay of Q^4 (RQ^4) to emphasize the differences between models, as this representation allows for better appreciation of the quality of the fit.[30] When fitting with the first model, where the PEDOT:PSS was split into two layers all three parameters (D, SLD, and σ_{RMS}) of the SiO_2 and the layer on top of the

SiO_2 (bottom polymer layer) were allowed to be fitted. For the top polymer layer only D and SLD were fitted and σ_{RMS} was constrained between the minimum and maximum values obtained by AFM. According to the best fit achieved the SiO_2 layer was 2.15 nm thick and had an σ_{RMS} of 1.01 nm, both within the common known ranges of a native oxide layer. The SLD was 3.15×10^{-6} Å^{-2} which is similar to the well known value of 3.47×10^{-6} Å^{-2} reported in literature,[40–42] confirming that this layer is a native oxide. Out of the two models used the bi-layer model had the best fit with a χ^2 of 2.95. The second model considered only one homogeneous PEDOT:PSS layer (similar to the one used to model the pristine sample) along with the fitting of its SLD and D, and the fitting the three parameters of the SiO_2 layer. The σ_{RMS} fitting of the PEDOT:PSS layer was again constrained to the AFM minimum and maximum values just as for the two layer model. The SiO_2 layer obtained with this model had an SLD of 3.6×10^{-6} Å^{-2}, was 2.3 nm thick, and had a σ_{RMS} of 1.7 nm. This model had a χ^2 of 3.6 which is 22% larger (worse) than the χ^2 of the 2 layer model. This improvement in the quality of the fit strongly suggests that the NR data of the 10 mM doped sample are best interpreted by assuming a separation of layers within the polymer film which would confirm the hypothesis described earlier in the paper.

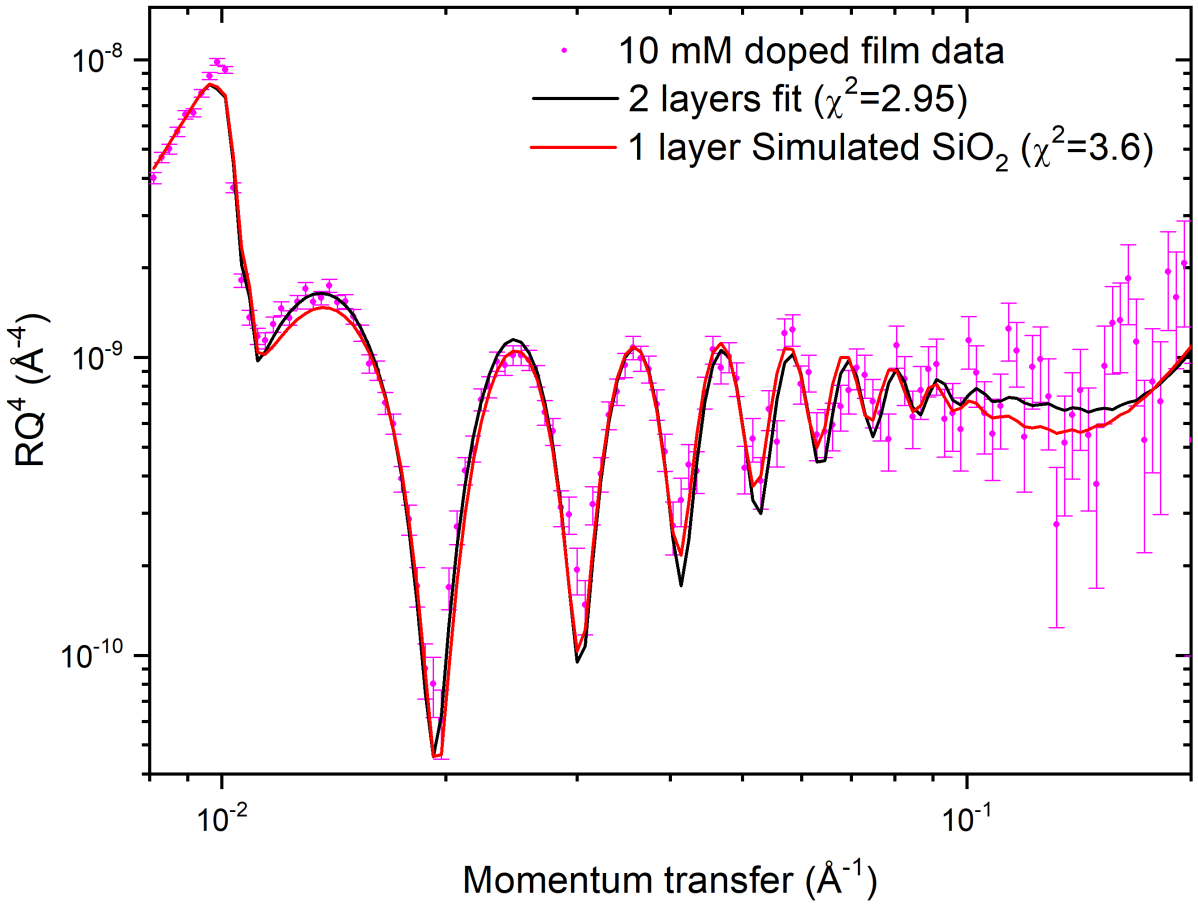

Figure 3: *Neutron reflectivity plotted as RQ^4 data for the 10 mM film and its corresponding fits using the two layer model (black) and the one layer model (red) both under same simulation conditions. The χ^2 values of each fit are shown for comparison evidencing a 22% improvement from the 1 layer model to the 2 layer model.*

The 20 mM doped sample was analyzed in the same way to investigate if this separation continues to occur as the doping concentration increases. The same types of models were applied to the 20 mM doped sample NR data, however, the results were different for this sample showing negligible improvement in the quality of the fit from the one layer model to the two layer model (see figure 4) with their χ^2 being almost identical (1.93 and 1.92 respectively). This suggests that for a doping level of 20 mM, the resulting film is a homogeneous mixed layer. The comparisons between the χ^2 of both models for the 10 mM and 20 mM are interesting as they suggest that at a lower level of DYMAP doping, the PEDOT:PSS:DYMAP deposited film separates into two layers, but forms a homogeneous

layer when the amount of zwitterion increases. We decided to further test the validity of this argument by applying a two layer model to the pristine sample and a three layer model to the 10 mM sample and found that there is not a significant improvement in the quality of the fit in such models (see supporting information S-4 to S-5). Additionally, we performed a second analysis for every model based on the Nevot-Croce scheme[43] and a different metric for the probabilistic evidence (see supporting information S-5 to S-15). The secondary analysis agrees with the findings reported in this section confirming that a one layer model for the pristine and the 20 mM samples, and a two layer model for the 10 mM sample are the most plausible interpretations for their polymer films.

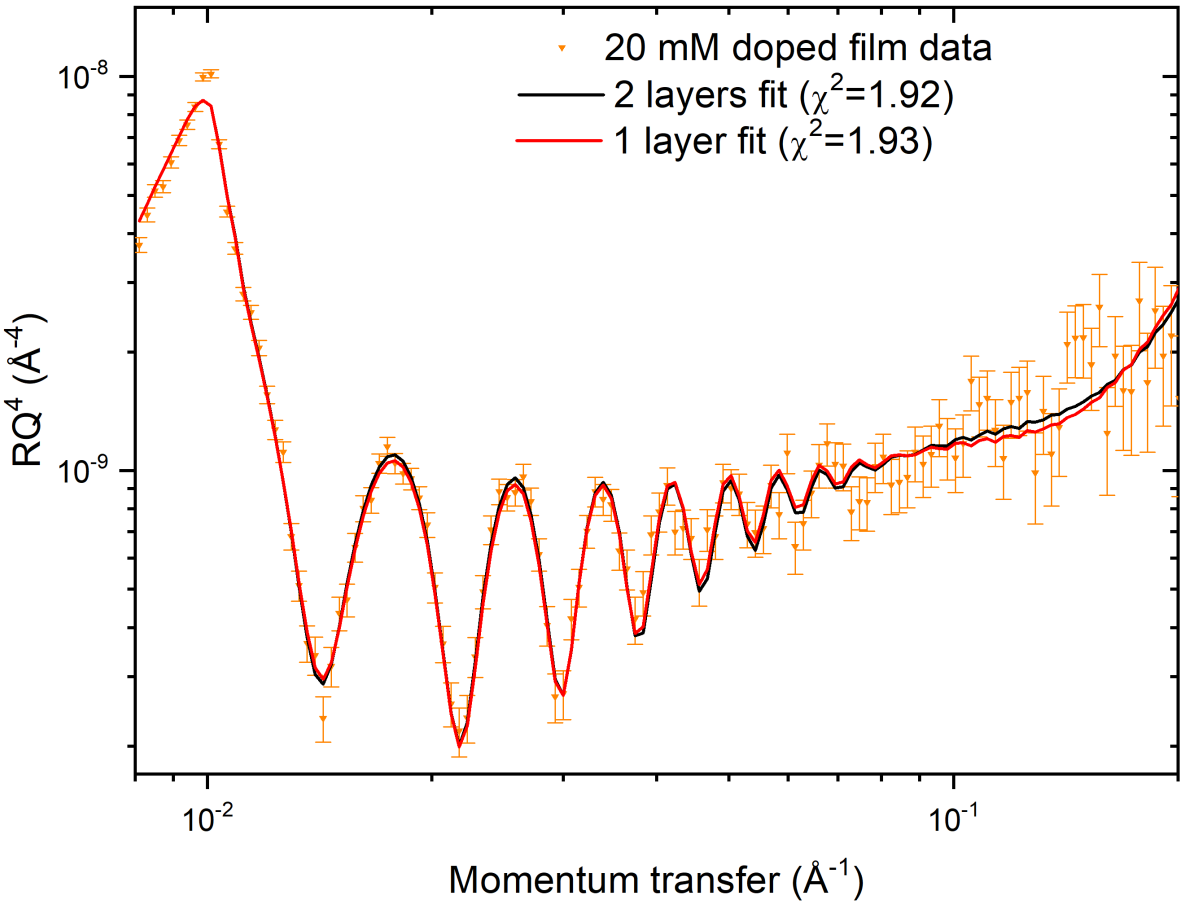

Figure 4: *Neutron reflectivity plotted as RQ^4 data for the 20 mM film and its corresponding fits using a two layer model (black), a one layer model (red) both under the same simulation conditions. The χ^2 values of each fit are shown for comparison of quality of fit evidencing that there is no significant improvement from using a two layer model over a one layer model (1% increase in quality of the fit).*

According to the two layer model for the 10 mM sample, there is a 10.1 nm thick layer on top of the SiO_2 with a σ_{RMS} of 8.1 nm. This is an unusually high σ_{RMS} to thickness ratio which indicates that this layer is not completely separated from the top layer, but rather going through a gradual separation. The SLD of the bottom layer was 1.1×10^{-6} Å^{-2} which is slightly lower than that of the undoped PEDOT:PSS film (see table 2). Given that the theoretical SLD value of DYMAP is 4.7×10^{-8} Å^{-2}, the decreased SLD of this bottom layer compared to that obtained for the pristine PEDOT:PSS suggests that the bottom polymer layer likely contains most of the DYMAP precipitated within the polymer film. The top polymer layer had a thickness of 45.86 nm, a σ_{RMS} of 1.15 nm, and an SLD of 1.37×10^{-6} Å^{-2} which is very similar to the one of the pristine sample. This implies that the top polymer layer is mostly comprised of undoped PEDOT:PSS with very small traces of DYMAP as indicated by a minimal decrease in SLD (from 1.42×10^{-6} Å^{-2} to 1.37×10^{-6} Å^{-2}). The total polymer film thickness of the 10 mM sample (bottom and top polymer layers combined) increased by 18% compared to the pristine sample, which hints at a swelling effect induced by DYMAP. As for the 20 mM sample 2 layer model, the bottom polymer layer had a thickness of 12.1 nm and a σ_{RMS} of 4.1 nm while the top polymer layer had a thickness of 65.7 nm and a σ_{RMS} of 0.96 nm. However the scattering length densities of both layers were very similar being 0.76 x 10^{-6} Å^{-2} for the bottom polymer and 0.82 x 10^{-6} Å^{-2} for the top polymer. This is a strong indication that the layers are not different from each other, supporting the argument that there is no separation of layers at this high concentration. For the 1 layer model the polymer layer was 78.02 nm thick and the σ_{RMS} was 0.96 nm. The SLD of the polymer layer was 8.0×10^{-7} Å^{-2} which if compared to the pristine PEDOT:PSS layer and the top layer of the 10 mM sample, is notably different (lower). This decrease in the SLD could be due to the modified density of the film caused by the dopant since it is 60% thicker compared to the pristine sample (see table 2). We must also add, however, that the same spin coating conditions were used throughout, but the solution became more viscous. Therefore an increase in thickness for the doped film

could also be caused by the spin coating process. Extracting quantitative results from two effects which have similar outcomes is therefore quite difficult. The increase in thickness of the PEDOT:PSS film caused by an asymmetrically charged dopant is an effect that is rarely considered in literature and has important implications on the interpretation of the morphology modifications of PEDOT:PSS. Moreover, it directly affects the measurement of its parameters such as efficiency in devices which is dependent on the thickness of the film,[44–46] and conductivity which is commonly obtained by measuring the sheet resistance and assuming a constant thickness for the pristine and the doped samples.

Figure 5 compares the scattering length density profiles of pristine (1 layer model), 10 mM (2 layer model) and 20 mM (1 layer model) DYMAP doped PEDOT:PSS.

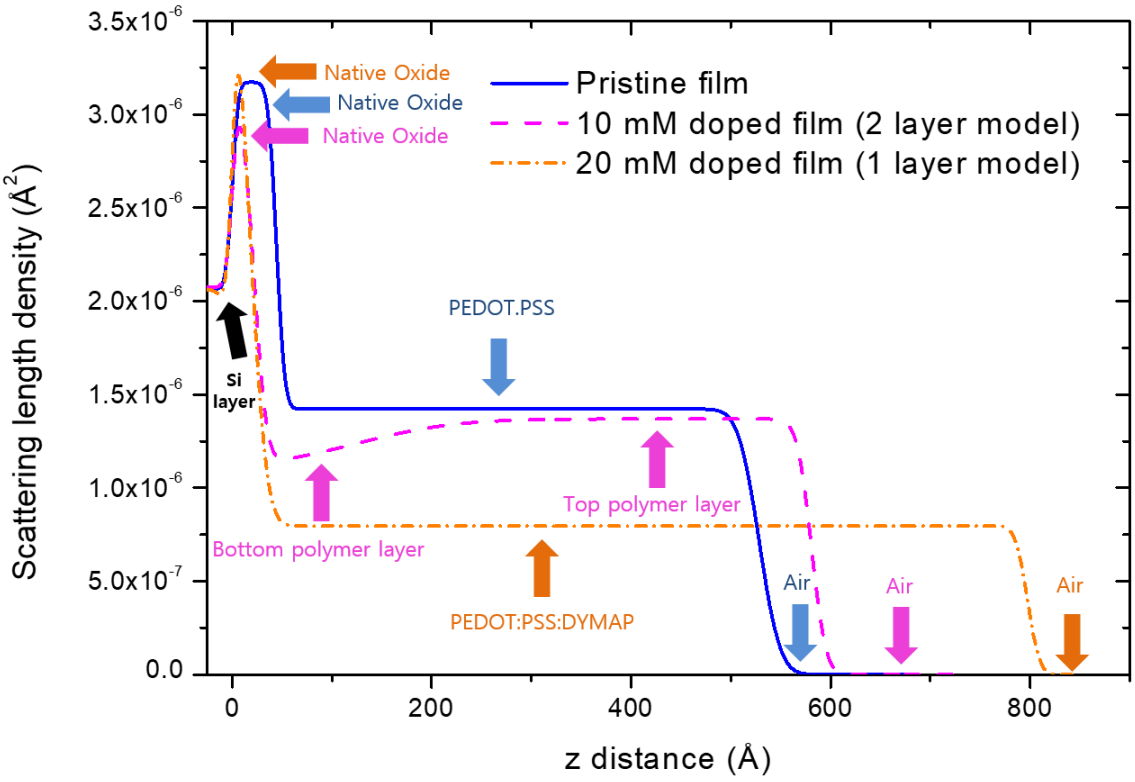

Figure 5: *Neutron scattering length density profiles of pristine, 10 mM(2 layer model), and 20 mM(1 layer model) DYMAP doped PEDOT(1):PSS(2.5).*

Given the results presented here, we propose that at lower doping concentration (e.g. 10 mM for DYMAP in PEDOT:PSS) the dopant preferentially accumulates close to the

substrate surface resulting in a bi-layer structure with the lower layer rich in the dopant (in this case DYMAP), and the top layer comprised of mostly undoped PEDOT:PSS. We think that reason why this happens is because at 10 mM the amount of DYMAP is insufficient to dope all of the PEDOT:PSS molecules. Subsequently, when this mix is processed into a thin film, separated layers form with the heavily doped layer near the Si interface. Moreover, the large effective roughness (relative to film thickness) of the bottom polymer suggests that this separation of layers is not into pure materials, in which one of them ceases to be at a specific point within the film's height. Instead, the film has a graded structure in which most of the dopant is found near the bottom of the film and its presence gradually decreases as a function of the film's height leaving the top of the film comprised of mostly PEDOT:PSS (see figures 6a and 6b). We also propose that when the dopant concentration increases (e.g. the 20 mM DYMAP doped PEDOT:PSS), the more evenly balanced PEDOT:PSS to dopant ratio allows the formation of a homogeneous film (see figures 6c and 6d). This is supported in our study by the resulting structure of the 20 mM DYMAP doped PEDOT:PSS from the NR data analysis.

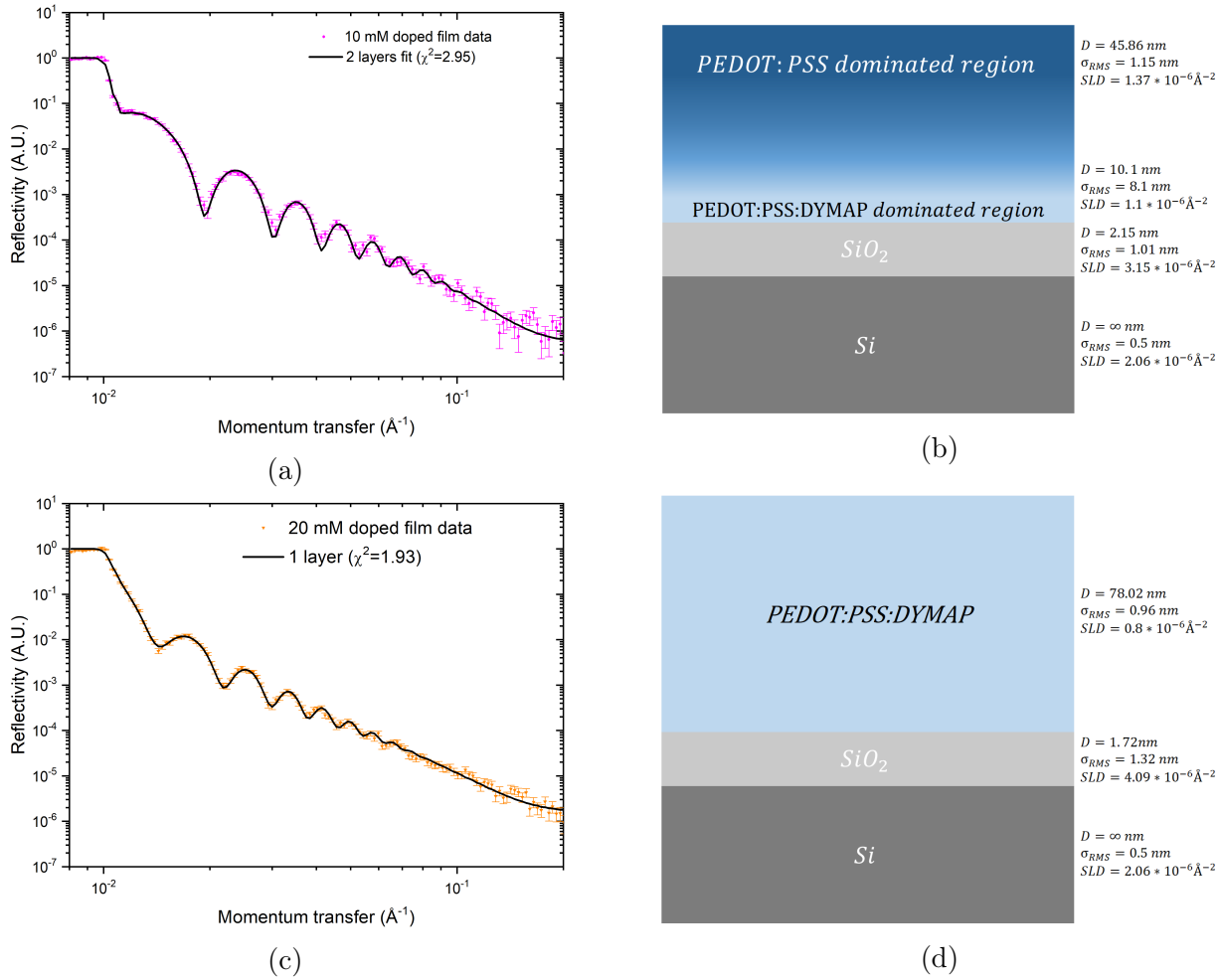

Figure 6: *Neutron reflectivity data for the 10 mM (a) and 20 mM (c) DYMAP doped PEDOT:PSS films and their corresponding chosen fits. The sketches of the 10 mM (b) and the 20 mM (d) samples (not to scale) are also shown along with their respective resulting values for thickness (D), root mean square roughness (σ_{RMS}), and scattering length density. (SLD)*

Table 2: *Thickness (D), root mean square roughness (σ_{RMS}), and scattering length density (SLD) of each sample by layer. The numbers shown for the 10 and 20 mM sample correspond to the 2 and 1 layer model respectively.*

Pristine

	D (nm)	σ_{RMS} (nm)	SLD (10^{-6}Å^{-2})
PEDOT:PSS	48.40	1.65	1.42
SiO_2	4.44	0.66	3.17

10 mM

	D (nm)	σ_{RMS} (nm)	SLD (10^{-6}Å^{-2})
Top Layer	45.86	1.15	1.37
Bottom Layer	10.1	8.10	1.10
SiO_2	2.15	1.01	3.15

20 Mm

	D (nm)	σ_{RMS} (nm)	SLD (10^{-6}Å^{-2})
PEDOT:PSS:DYMAP	78.02	0.96	0.80
SiO_2	1.72	1.32	4.09

2.3 Atomic Force Microscopy

In order to aid the NR data analysis by determining the σ_{RMS} and to study the surface morphology of the films, AFM was conducted. The results can be compared in table 3

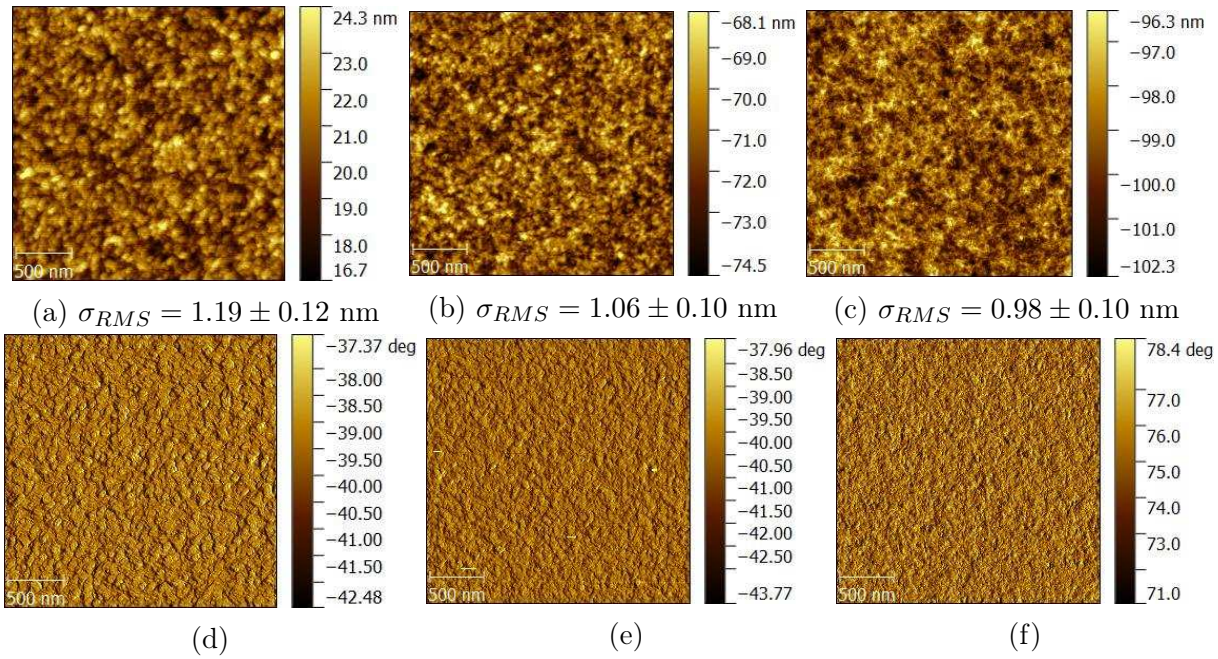

(a) $\sigma_{RMS} = 1.19 \pm 0.12$ nm (b) $\sigma_{RMS} = 1.06 \pm 0.10$ nm (c) $\sigma_{RMS} = 0.98 \pm 0.10$ nm

(d) (e) (f)

Figure 7: *AFM height (top) and phase (bottom) images of pristine PEDOT:PSS (a and d), and 10 mM (b and e) and 20 mM (c and f) DYAMP doped PEDOT:PSS. Images show decreasing root mean squared roughness as the dopant concentration increases.*

Height and phase images are presented in figure 7. The pristine sample (7a and 7d) had an average σ_{RMS} of 1.19, the highest of all samples. Figure 7 also shows that there are clear nodules (spherical features) in the height image which have been identified before as PEDOT aggregates.[25] As the concentration increases it can be appreciated how those nodules tend to disappear or dissipate and instead a more interconnected film network is formed. This observation is also supported by the subtle decrease in the average roughness of the 10 and 20 mM samples which are 1.07 nm and 0.96 nm respectively, as it is known that PEDOT is a rough polymer when deposited as a thin film.[26] This trend supports the argument presented in the NR analysis section where it is observed that at a low concentration of DYMAP the surface layer is mostly PEDOT:PSS with minor traces of DYMAP. However as the doping concentration increases, the DYMAP becomes better mixed through all PEDOT:PSS and the resulting surface morphology is considerably different in comparison to the pristine sample being smoother and less aggregated. This change in surface morphology can also be seen in the phase images (figures 7d, 7e, and 7f) where the 20 mM sample looks more homogeneous

than the 10 mM and pristine samples supporting the idea described in the NR section of the surface of the film transitioning from PEDOT:PSS to PEDOT:PSS:DYMAP as the dopant concentration increases.

Table 3: *Root mean square roughness (σ_{RMS} and thickness (D) values of the pristine, 10 mM, and 20 mM DYMAP doped PEDOT:PSS samples obtained by surface measurement techniques (AFM and profilometer) and neutron reflectivity modeling.*

	$\sigma_{RMS}(nm)$		$D(nm)$	
	NR	AFM	NR	Profilometer
Pristine	1.65	1.19±0.12	48.40	48.0±0.8
10 mM	1.15	1.06±0.10	55.96	58.3±4.5
20 mM	0.96	0.98±0.10	78.02	90.3±5.7

2.4 Device performance

Finally DYMAP doped PEDOT:PSS films were incorporated into organic photovoltaic devices to test their performance and to test if doping the PEDOT:PSS brings any improvement to the device. The films were incorporated as the HTL in PCDTBT:$PC_{71}BM$ based devices. We were expecting to see an increase in the power conversion efficiency (PCE) of the 20 mM sample since its conductivity is significantly increased (by one order of magnitude) compared to the pristine and the 10 mM sample (see supporting information S-15 to S-18). However, not only the overal PCE of the devices went down, but all the other photovoltaic parameters decreased as well. We attributed this decrease in performance to the increased phobic behavior of the doped samples towards the active layer solvent. We suggest that such phobic behaviour hinders the quality of the contact between the HTL and the active layer due to dewetting (see supporting information Figure S9).

3 Conclusions

The structural and electronic properties of DYMAP doped PEDOT:PSS films depends strongly upon the concentration of DYMAP used. The un-doped PEDOT:PSS forms a

uniform thin film with some evidence of PEDOT aggregates on the surface. Upon doping, the film thickness increases and at low concentration the DYMAP preferentially segregates towards the substrate resulting in two layers with a graded interface after film deposition. The bottom polymer layer is comprised of DYMAP doped PEDOT:PSS and the top polymer layer is mostly comprised of PEDOT:PSS with negligible traces of the zwitterion. The roughness of the interface between these two layers suggests that across the interface, the zwitterion content decreases as a function of height within the film. This separation into two layers only occurs at the low zwitterion to PEDOT:PSS ratio, as when the concentration of DYMAP is further increased the NR data shows complete intermixing of the PEDOT:PSS with the zwitterion resulting in a homogeneously mixed film. The AFM results indicate a change in surface morphology from rough to smooth, with fewer PEDOT aggregates on the top surface as it changes from PEDOT:PSS to PEDOT:PSS:DYMAP. The homogeneous 20 mM PEDOT:PSS:DYMAP films have a significantly higher conductivity, by over an order of magnitude ($\sim$20-50 times) compared to the intermediate 10 mM films and the pristine PEDOT:PSS. The later two had similar conductivities with the 10 mM films showing a similar surface texture and only a slight reduction in conductivity compared to the pristine PEDOT:PSS. When incorporated as HTLs in PCDTBT:PC71BM in OSC devices we found that the photovoltaic performance decreases as the concentration of DYMAP in PEDOT:PSS increases. Therefore it is clear that addition of zwitterion as a dopant in PEDOT:PSS results in complex concentration dependent changes that influence the morphological and electronic properties of the films. Understanding this complex relationship goes some way to explaining the discrepancies reported in the literature regarding the effectiveness of using dopants in PEDOT:PSS.

4 Experimental

4.1 Materials

PCDTBT, $PC_{71}BM$ (95% purity), encapsulation epoxy, and PEDOT:PSS in aqueous dispersion (HTL Solar) for which the solid content is in between 1.0 and 1.2 wt% and the PEDOT to PSS ratio is 1:2.5, were all purchased from Ossila. DYMAP ($\geq$ 98% purity) was purchased from Sigma Aldrich. All chemicals were used without further purification or treatment. Encapsulation glass slides and indium tin oxide (ITO) glass pixelated cathode substrates (6 pixels) were also purchased from Ossila and were used for device fabrication. Menzel-Gläser microscope glass slides were used as substrates for the PEDOT:PSS:DYMAP films that were subject to four point probe (FPP) sheet resistance characterization and profilometry measurements, while 425 μm P/Boron doped polished silicon wafers purchased from Si-Mat were used as the substrate for the films that were subject to AFM measurements. Polished 4 mm thick circular silicon wafers (50 mm in diameter) were used to support the films that were characterized with NR and were purchased from Prolog Semicor Ltd.

4.2 Film preparation and device fabrication

All types of substrate were washed in an ultrasonic bath at 60°C for 10 minutes in a 1% Hellmanex ™III/deionized water solution and subsequently in 2-Propanol. After each sonication the substrates were rinsed twice in hot D.I. water and once in cold D.I. water. The substrates were then dried by a nitrogen gas flow and then they were cleaned with oxygen plasma for 5 minutes. PEDOT:PSS dispersion was taken out of storage at 4°C and 4 mL filtered through a 0.45 μm polyvinyl difluoride syringe filter into a clean amber vial. 3.6 mg and 7.2 mg of DYMAP were put in three different amber vials and then 1 mL of the filtered PEDOT:PSS solution was added to each of the vials to obtain the 10 and 20 mM PEDOT:PSS:DYMAP concentrated solutions. All three solutions (the two different doping concentrations and the undoped one) were then sonicated for 5 minutes prior to use. The

solutions were spun-cast onto the substrates at 4000 RPM for 40 s and then annealed at 150°C for 15 minutes. The films were subsequently left to cool down to room temperature prior to any measurement or further device fabrication process. All these procedures were conducted in ambient conditions. For neutron reflectivity and profilometry measurements the films were measured more than 24 hours after their preparation to allow them to reach maximum ambient water absorption. This was done in order to minimize ambient water absorption from the films during neutron reflectivity measurements which could compromise the accuracy of the data. For device fabrication the annealed PEDOT:PSS films on the ITO substrates were subsequently coated with a 1:4 PCDTBT:$PC_{71}BM$ ratio blend solution dissolved in chlorobenzene. This solution was prepared by stirring a 4 mg/mL solution of PCDTBT in chlorobenzene overnight at 70 °C and then adding 16 mg of $PC_{71}BM$ to the solution with continued stirring for 2 additional hours at the same temperature. The solution was filtered with a 0.45 μm polytetrafluoroethylene filter before use. The coating speed and time for this film was 700 RPM for 30 seconds. Aluminium electrodes were then thermally evaporated onto the devices through a shadow mask with an aluminium deposition rate between 0.5 and 1 nm/s for the first 50 nm and then at a rate between 4 and 8 nm/s for the rest of the total 166 nm thick film. The samples were then encapsulated using epoxy and glass coverslips and cured with UV light for 10 minutes.

4.3 Measurements and characterization

The neutron reflectivity data were obtained at the ISIS neutron and muon source (Oxfordshire, UK) using the OFFSPEC reflectometer, which has an incident neutron wavelength range from 1.5 Åto 14 Å. Reflectivity data were collected at three different angles (0.4° , 0.9°, and 2.3°) to cover the required momentum transfer range (0.08 to 0.25 $Å^{-1}$). The data were then analyzed with the software GenX using the soft nx model.[47] The conductivity of the films was calculated using their sheet resistance and thickness values (see supporting information S-2). Sheet resistance was measured using a FPP system (see supporting infor-

mation table S1) incorporating a Keithley 2602 source measurement unit. The thickness of the films for the conductivity measurements was obtained with a J.A. Woollam Co. M-2000 ellipsometer with detector (charge-coupled devices, CCD camera) and a Cauchy model fitted in the CompleateEase software by J.A. Woolam. Film thickness for comparison with the neutron reflectivity data was measured across a scratch with a Bruker DektakXT profilometer (12.5μm stylus radius) and the Vision64 software (0.33μm/pt scan resolution). AFM images and roughness measurements were obtained with a Veeco Dimension 3100 AFM with a NanoScope IV controller and a TESPA-V2 cantilever (37N/m nominal stiffness and 320 kHz nominal resonance frequency) in tapping mode. Contact angle values were obtained with a Theta Lite Basic kit and integrated software (accuracy of $\pm 0.1^{\circ}$) from Nima (now Biolin Scientific). The performance of the photovoltaic devices was measured using a Newport 92251A-1000 solar simulator (AM 1.5) calibrated for the combined light output to 100 mW cm^{-2} at 25°C. An aperture mask (six apertures of 0.025 cm^2 for six different and evenly distributed measurements within the surface of the device) was placed on top of the devices to define the active area during the voltage sweep. The photovoltaic parameters were subsequently calculated from the J-V curve and the illuminated intensity.

Acknowledgement

G.P thanks the National Council of Science and Technology (CONACyT) of Mexico and the Mexico Secretary of Energy (SENER) for the provision of a PhD scholarship. A.D. wishes to acknowledge support from the EPSRC through Supergen Solar Challenge Grant : EP/M025020/1. G.B. thanks the Eurpean comission for a Marie Sklodowska Curie Individual Fellowship (FP7/H2020 ®Grant agreement number: 658391). We also gratefully acknowledge Prof Gregory Beaucage for helpful discussions and the Science and Technology Facilities Council (STFC) for access to neutron beamtime at ISIS on Offspec (RB:1710397, DOI:10.5286/ISIS.E.84794745), and also for the provision of sample preparation facilities.

Supporting Information Available

The following files are available free of charge.

- Filename: S.I. NR. Contains: details on the calculation of conductivity (page S-2), sheet resistance and thickness values of films (Table S1), abnormally thick SiO_2 layer discussion (pages S-2 and S-3), ellipsometry graph (Figure S1a) and AFM height image (Figure S1b) of the abnormally thick SiO_2 layer, additional validation of the quality of the fit argument (pages S-4 and S-5), data and fits plotted as RQ^4 of the pristine (2 layers) and 20 mM (3 layer) samples (Figure S2), parameters resulting from the 2 layer and 3 layer models for the pristine and 10 mM samples respectively (Table S2), secondary analysis of the neutron reflectivity data (pages S-5 to S-15), secondary analysis data, fits, and parameters in GenX for the pristine (Figures S3 and S4), 10 mM (Figures S5, S6, and S7), and 20 mM (Figures S8, s9, and S10) samples, parameters of the secondary analysis models for the pristine (Table S3,) 10 mM (Table S4), and 20 mM (Table S5), device performance discussion (pages S-15 to S-18), photovoltaic performance and I-V curves of devices (Figure S11), and contact angle images of the films (Figure S12).

References

(1) Po, R.; Carbonera, C.; Bernardi, A.; Camaioni, N. The Role of Buffer Layers in Polymer Solar Cells. *Energy Environ. Sci.* **2011**, *4*, 285–310.

(2) Lattante, S. Electron and Hole Transport Layers: Their Use in Inverted Bulk Heterojunction Polymer Solar Cells. *Electronics* **2014**, *3*, 132–164.

(3) Dietrich, M.; Heinze, J.; Heywang, G.; Jonas, F. Electrochemical and Spectroscopic Characterization of Polyalkylenedioxythiophenes. *J. Electroanal. Chem.* **1994**, *369*, 87–92.

(4) Hokazono, M.; Anno, H.; Toshima, N. Thermoelectric Properties and Thermal Stability of PEDOT:PSS Films on a Polyimide Substrate and Application in Flexible Energy Conversion Devices. *J. Electron. Mater.* **2014**, *43*, 2196–2201.

(5) Cho, C.-K.; Hwang, W.-J.; Eun, K.; Choa, S.-H.; Na, S.-I.; Kim, H.-K. Mechanical Flexibility of Transparent PEDOT:PSS Electrodes Prepared by Gravure Printing for Flexible Organic Solar Cells. *Sol. Energy Mater Sol. Cells* **2011**, *95*, 3269 – 3275.

(6) Vitoratos, E.; Sakkopoulos, S.; Dalas, E.; Paliatsas, N.; Karageorgopoulos, D.; Petraki, F.; Kennou, S.; Choulis, S. Thermal Degradation Mechanisms of PEDOT:PSS. *Org. Electron.* **2009**, *10*, 61–66.

(7) Groenendaal, L.; Jonas, F.; Freitag, D.; Pielartzik, H.; Reynolds, J. R. Poly(3,4-ethylenedioxythiophene) and its Derivatives: Past, Present, and Future. *Adv. Mater.* **2000**, *12*, 481–494.

(8) Irwin, M. D.; Buchholz, D. B.; Hains, A. W.; Chang, R. P. H.; Marks, T. J. p-Type Semiconducting Nickel Oxide as an Efficiency-Enhancing Anode Interfacial Layer in Polymer Bulk-heterojunction Solar Cells. *Proc. Natl. Acad. Sci. U.S.A.* **2008**, *105*, 2783–2787.

(9) Li, G.; Chu, C.-W.; Shrotriya, V.; Huang, J.; Yang, Y. Efficient Inverted Polymer Solar Cells. *Appl. Phys. Lett.* **2006**, *88*.

(10) Zhao, Z.; Zhang, W.; Zhao, X.; Yang, S. *Organic Solar Cells materials, devices, interfaces, and modeling*; Boca Raton: CRC Press, 2015; London.

(11) Yang, J.; Oh, S.; Kim, D.; Kim, S.; Kim, H. Hole Transport Enhancing Effects of Polar Solvents on Poly(3,4- ethylenedioxythiophene):Poly(styrene sulfonic acid) for Organic Solar Cells. *ACS Appl. Mater. Interfaces* **2012**, *4*, 5394–5398.

(12) Hu, Z.; Zhang, J.; Hao, Z.; Zhao, Y. Influence of Doped PEDOT:PSS on the Performance of Polymer Solar Cells. *Sol. Energy Mater Sol. Cells* **2011**, *95*, 2763 – 2767.

(13) Alemu, D.; Wei, H.-Y.; Ho, K.-C.; Chu, C.-W. Highly Conductive PEDOT:PSS Electrode by Simple Film Treatment with Methanol for ITO-Free Polymer Solar Cells. *Energy Environ. Sci.* **2012**, *5*, 9662–9671.

(14) Girotto, C.; Moia, D.; Rand, B.; Heremans, P. High-Performance Organic Solar Cells with Spray-Coated Hole-Transport and Active Layers. *Adv. Funct. Mater.* **2011**, *21*, 64–72.

(15) Dobbelin, M.; Marcilla, R.; Salsamendi, M.; Pozo-Gonzalo, C.; Carrasco, P.; Pomposo, J.; Mecerreyes, D. Influence of Ionic Liquids on the Electrical Conductivity and Morphology of PEDOT:PSS Films. *Chem. Mater.* **2007**, *19*, 2147–2149.

(16) Kwak, C. K.; Pérez, G. E.; Freestone, B. G.; Al-Isaee, S. A.; Iraqi, A.; Lidzey, D. G.; Dunbar, A. D. F. Improved Efficiency in Organic Solar Cells Via Conjugated Polyelectrolyte Additive in the Hole Transporting Layer. *J. Mater. Chem. C* **2016**, *4*, 10722–10730.

(17) Xia, Y.; Ouyang, J. Significant Conductivity Enhancement of Conductive Poly(3,4-ethylenedioxythiophene):Poly(styrenesulfonate) Films Through a Treatment with Organic Carboxylic Acids and Inorganic Acids. *ACS Appl. Mater. Interfaces* **2010**, *2*, 474–483.

(18) Lin, C.-C.; Huang, C.-K.; Hung, Y.-C.; Chang, M.-Y. Enhanced Conductivity of Poly(3,4-ethylenedioxythiophene):Poly(styrene sulfonate) Film by Acid Treatment for Indium Tin Oxide-Free Organic Solar Cells. *Jpn. J. Appl. Phys.* **2016**, *55*, 081602.

(19) Fang, G.; Wu, S.; Xie, Z.; Geng, Y.; Wang, L. Enhanced Performance for Polymer Solar Cells by Using Surfactant-Modified PEDOT:PSS as the Anode Buffer Layer. *Macromol. Chem. Phys.* **2011**, *212*, 1846–1851.

(20) Zhao, Z.; Wu, Q.; Xia, F.; Chen, X.; Liu, Y.; Zhang, W.; Zhu, J.; Dai, S.; Yang, S. Improving the Conductivity of PEDOT:PSS Hole Transport Layer in Polymer Solar Cells via Copper(II) Bromide Salt Doping. *ACS Appl. Mater. Interfaces* **2015**, *7*, 1439–1448.

(21) Xia, Y.; Ouyang, J. Anion Effect on Salt-Induced Conductivity Enhancement of Poly(3,4-ethylenedioxythiophene):Poly(styrenesulfonate) Films. *Org. Electron.* **2010**, *11*, 1129–1135.

(22) Xia, Y.; Ouyang, J. Salt-induced Charge Screening and Significant Conductivity Enhancement of Conducting Poly(3,4-ethylenedioxythiophene):Poly(styrenesulfonate). *Macromolecules* **2009**, *42*, 4141–4147.

(23) Fan, Z.; Du, D.; Yu, Z.; Li, P.; Xia, Y.; Ouyang, J. Significant Enhancement in the Thermoelectric Properties of PEDOT:PSS Films Through a Treatment with Organic Solutions of Inorganic Salts. *ACS Appl. Mater. Interfaces* **2016**, *8*, 23204–23211.

(24) Xia, Y.; Zhang, H.; Ouyang, J. Highly Conductive PEDOT:PSS Films Prepared Through a Treatment with Zwitterions and Their Application in Polymer Photovoltaic Cells. *J. Mater. Chem.* **2010**, *20*, 9740–9747.

(25) Zhao, Z.; Chen, X.; Liu, Q.; Wu, Q.; Zhu, J.; Dai, S.; Yang, S. Efficiency Enhancement of Polymer Solar Cells via Zwitterion Doping in PEDOT:PSS Hole Transport Layer. *Org. Electron.* **2015**, *27*, 232–239.

(26) Ouyang, J. "Secondary Doping" Methods to Significantly Enhance the Conductivity of PEDOT:PSS for its Application as Transparent Electrode of Optoelectronic Devices. *Displays* **2013**, *34*, 423–436.

(27) Kim, J.; Jung, J.; Lee, D.; Joo, J. Enhancement of Electrical Conductivity of Poly(3,4-ethylenedioxythiophene)/Poly(4-styrenesulfonate) by a Change of Solvents. *Synth. Met.* **2002**, *126*, 311–316.

(28) Xia, Y.; Ouyang, J. PEDOT:PSS Films with Significantly Enhanced Conductivities Induced by Preferential Solvation with Cosolvents and Their Application in Polymer Photovoltaic Cells. *J. Mater. Chem.* **2011**, *21*, 4927–4936.

(29) Crispin, X.; Jakobsson, F.; Crispin, A.; Grim, P.; Andersson, P.; Volodin, A.; Van Haesendonck, C.; Van Der Auweraer, M.; Salaneck, W.; Berggren, M. The Origin of the High Conductivity of Poly(3,4-ethylenedioxythiophene)-Poly(styrenesulfonate) (PEDOT-PSS) Plastic Electrodes. *Chem. Mater.* **2006**, *18*, 4354–4360.

(30) Parnell, A.; Dunbar, A.; Pearson, A.; Staniec, P.; Dennison, A.; Hamamatsu, H.; Skoda, M.; Lidzey, D.; Jones, R. Depletion of PCBM at the Cathode Interface in P3HT/PCBM Thin Films as Quantified via Neutron Reflectivity Measurements. *Adv. Mater* **2010**, *22*, 2444–2447.

(31) Ma, W.; Yang, C.; Gong, X.; Lee, K.; Heeger, A. J. Thermally Stable, Efficient Polymer Solar Cells with Nanoscale Control of the Interpenetrating Network Morphology. *Adv. Funct. Mater.* **2005**, *15*, 1617–1622.

(32) Veder, J.; Patel, K.; Sohail, M.; Jiang, S.; James, M.; DeMarco, R. An Electrochemical Impedance Spectroscopy/Neutron Reflectometry Study of Water Uptake in the Poly(3,4-Ethylenedioxythiophene):Poly(Styrene Sulfonate)/Polymethyl Methacrylate-Polydecyl Methacrylate Copolymer Solid-Contact Ion-Selective Electrode. *Electroanalysis* **2012**, *24*, 140–145.

(33) Rodríguez, A.; Voigt, M.; Martin, S.; Whittle, T.; Dalgliesh, R.; Thompson, R.; Lidzey, D.; Geoghegan, M. Structure of Films of Poly(3,4-ethylene dioxythiophene)-Poly(styrene sulfonate) Crosslinked with Glycerol. *J. Mater. Chem.* **2011**, *21*, 19324–19330.

(34) Mauger, S.; Li, J.; Özmen, Ö.; Yang, A.; Friedrich, S.; Rail, M.; Berben, L.; MoulÃĺ, A.

High Work-Function Hole Transport Layers by Self-Assembly Using a Fluorinated Additive. *J. Mater. Chem. C* **2014**, *2*, 115–123.

(35) Kim, J.; Jung, J.; Lee, D.; Joo, J. Enhancement of Electrical Conductivity of Poly(3,4-ethylenedioxythiophene)/Poly(4-styrenesulfonate) by a Change of Solvents. *Synth. Met.* **2002**, *126*, 311 – 316.

(36) Lee, C.; Kim, J.; Lee, D.; Koo, Y.; Joo, J.; Han, S.; Beag, Y.; Koh, S. Organic Based Flexible Speaker Through Enhanced Conductivity of PEDOT/PSS with Various Solvents. *Synth. Met.* **2003**, *135-136*, 13–14.

(37) Kwak, C. New Challenges in Environmentally Friendly Materials for Organic and Perovskite Photovoltaic Cells. Ph.D. thesis, The Univesrity of Sheffield, 2016.

(38) Pavlopoulou, E.; Fleury, G.; Deribew, D.; Cousin, F.; Geoghegan, M.; Hadziioannou, G. Phase Separation-Driven Stratification in Conventional and Inverted P3HT:PCBM Organic Solar Cells. *Org. Electron.* **2013**, *14*, 1249–1254.

(39) Sivia, D.; Webster, J. The Bayesian Approach to Reflectivity Data. *Physica B: Condens. Matter* **1998**, *248*, 327–337.

(40) Wang, W.; Metwalli, E.; Perlich, J.; Papadakis, C.; Cubitt, R.; Müller-Buschbaum, P. Cyclic Switching of Water Storage in Thin Block Copolymer Films Containing Poly (N-isopropylacrylamide). *Macromolecules* **2009**, *42*, 9041–9051.

(41) Zhong, Q.; Metwalli, E.; Rawolle, M.; Kaune, G.; Bivigou-Koumba, A. M.; Laschewsky, A.; Papadakis, C. M.; Cubitt, R.; Müller-Buschbaum, P. Rehydration of Thermoresponsive Poly (monomethoxydiethylene glycol acrylate) Films Probed in Situ by Real-Time Neutron Reflectivity. *Macromolecules* **2015**, *48*, 3604–3612.

(42) Zhong, Q.; Metwalli, E.; Rawolle, M.; Kaune, G.; Bivigou-Koumba, A. M.; Laschewsky, A.; Papadakis, C. M.; Cubitt, R.; Wang, J.; Müller-Buschbaum, P. Influ-

ence of Hydrophobic Polystyrene Blocks on the Rehydration of Polystyrene-block-poly (methoxy diethylene glycol acrylate)-block-polystyrene Films Investigated by in Situ Neutron Reflectivity. *Macromolecules* **2015**, *49*, 317–326.

(43) Nevot, L.; Croce, P. Caractérisation des Surfaces par Réflexion Rasante de Rayons X. Application à l'étude du Polissage de Quelques Verres Silicates. *Rev. Phys. Appl.* **1980**, *15*, 761–779.

(44) Kim, Y.; Ballantyne, A. M.; Nelson, J.; Bradley, D. D. Effects of Thickness and Thermal Annealing of the PEDOT:PSS Layer on the Performance of Polymer Solar Cells. *Org. Electron.* **2009**, *10*, 205 – 209.

(45) Friedel, B.; Keivanidis, P.; Brenner, T.; Abrusci, A.; McNeill, C.; Friend, R.; Greenham, N. Effects of Layer Thickness and Annealing of PEDOT:PSS Layers in Organic Photodetectors. *Macromolecules* **2009**, *42*, 6741–6747.

(46) Wang, Y.; Luo, Q.; Wu, N.; Wang, Q.; Zhu, H.; Chen, L.; Li, Y.-Q.; Luo, L.; Ma, C.-Q. Solution-Processed MoO_3:PEDOT:PSS Hybrid Hole Transporting Layer for Inverted Polymer Solar Cells. *ACS Appl. Mater. Interfaces* **2015**, *7*, 7170–7179.

(47) Voegeli, W.; Kamezawa, C.; Arakawa, E.; Yano, Y. F.; Shirasawa, T.; Takahashi, T.; Matsushita, T. A Quick Convergent-Beam Laboratory X-ray Reflectometer Using a Simultaneous Multiple-Angle Dispersive Geometry. *J. Appl. Crystallogr.* **2017**, *50*, 570–575.

Graphical TOC Entry